analytical chemistry

Article

Cite This: *Anal. Chem.* 2018, 90, 3299−3306

pubs.acs.org/ac

High-Speed Live-Cell Interferometry: A New Method for Quantifying Tumor Drug Resistance and Heterogeneity

Dian Huang,[†] Kevin A. Leslie,[‡] Daniel Guest,[‡] Olga Yeshcheulova,[‡] Irena J. Roy,[§] Marco Piva,[∥] Gatien Moriceau,[∥] Thomas A. Zangle,[⊥] Roger S. Lo,[∥,#,▽] Michael A. Teitell,*[,†,§,▽,○] and Jason Reed*[,‡,◆]

[†]Department of Bioengineering, [§]Department of Pathology and Laboratory Medicine, [∥]Division of Dermatology, Department of Medicine, [#]Department of Molecular and Medical Pharmacology, [▽]Jonsson Comprehensive Cancer Center, and [○]Broad Stem Cell Research Center, California NanoSystems Institute, and Molecular Biology Institute, University of California, Los Angeles, California 90095, United States

[‡]Department of Physics, Virginia Commonwealth University, Richmond, Virginia 23284, United States

[⊥]Department of Chemical Engineering, University of Utah, Salt Lake City, Utah 84112, United States

[◆]Massey Cancer Center, Virginia Commonwealth University, Richmond, Virginia 23298, United States

Supporting Information

ABSTRACT: We report the development of high-speed live-cell interferometry (HSLCI), a new multisample, multidrug testing platform for directly measuring tumor therapy response via real-time optical cell biomass measurements. As a proof of concept, we show that HSLCI rapidly profiles changes in biomass in BRAF inhibitor (BRAFi)-sensitive parental melanoma cell lines and in their isogenic BRAFi-resistant sublines. We show reproducible results from two different HSLCI platforms at two institutions that generate biomass kinetic signatures capable of discriminating between BRAFi-sensitive and -resistant melanoma cells within 24 h. Like other quantitative phase imaging (QPI) modalities, HSLCI is well-suited to noninvasive measurements of single cells and cell clusters, requiring no fluorescence or dye labeling. HSLCI is substantially faster and more sensitive than field-standard growth inhibition assays, and in terms of the number of cells measured simultaneously, the number of drugs tested in parallel, and temporal measurement range, it exceeds the state of the art by more than 10-fold. The accuracy and speed of HSLCI in profiling tumor cell heterogeneity and therapy resistance are promising features of potential tools to guide patient therapeutic selections.

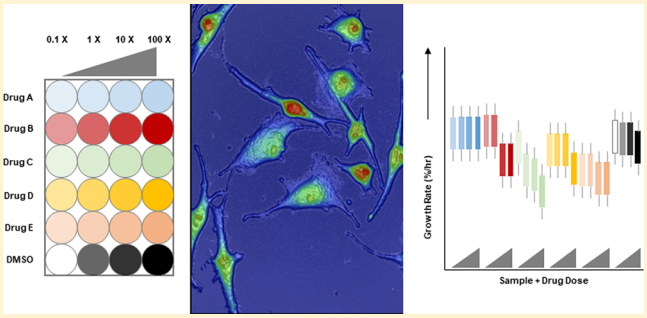

Prompt and repeated assessments of tumor sensitivity to available therapeutics could dramatically improve cancer patients' clinical outcomes by staying ahead of developing therapy resistance. However, to achieve this goal, substantial improvements in the state of the art will be required to create effective and practical therapy selection tools that rely on live-cell and tissue responses. There are a number of relevant performance measurables with which to evaluate live-cell drug response assays. These include (a) the number of drugs or drug combinations tested simultaneously, (b) the overall depth of sampling (i.e., the number of individual cells measured), and (c) the achievable duration of high-quality measurements. The present study describes a new technique, high-speed live-cell interferometry (HSLCI), that is based on rapid optical cell biomass measurements and, as quantified by the metrics mentioned, exceeds the current field standard by greater than 10-fold. Here we apply HSLCI as a proof of concept to metastatic melanoma, a disease in which tumor heterogeneity and drug resistance are significant obstacles to survival benefits from mutation-targeted therapy. Our results support the potential of HSLCI as a therapy selection tool, for dissecting overall tumor heterogeneity, and for predicting single-cell drug resistance and treatment outcomes, and we argue for further development of this technology in preclinical animal tests and early-phase clinical trials.

An estimated 87 110 new cases of cutaneous melanoma with 9730 deaths will occur for the United States in 2017.[1] Despite comprising less than 2% of skin cancer diagnoses,[2] melanoma is responsible for 75% of skin cancer deaths. Genetic landscape studies show interpatient, intrapatient, and intratumor heterogeneity. About 50% of melanomas harbor an activating mutation in the *BRAF* gene, whereas 10−25% of cases show an activating *RAS* mutation, 12−18% are mutant in *NF1*, and 7−28% of tumors show mutations in genes that include *AKT*

Received: November 21, 2017
Accepted: January 30, 2018
Published: January 30, 2018

ACS Publications © 2018 American Chemical Society

DOI: 10.1021/acs.analchem.7b04828
Anal. Chem. 2018, 90, 3299−3306

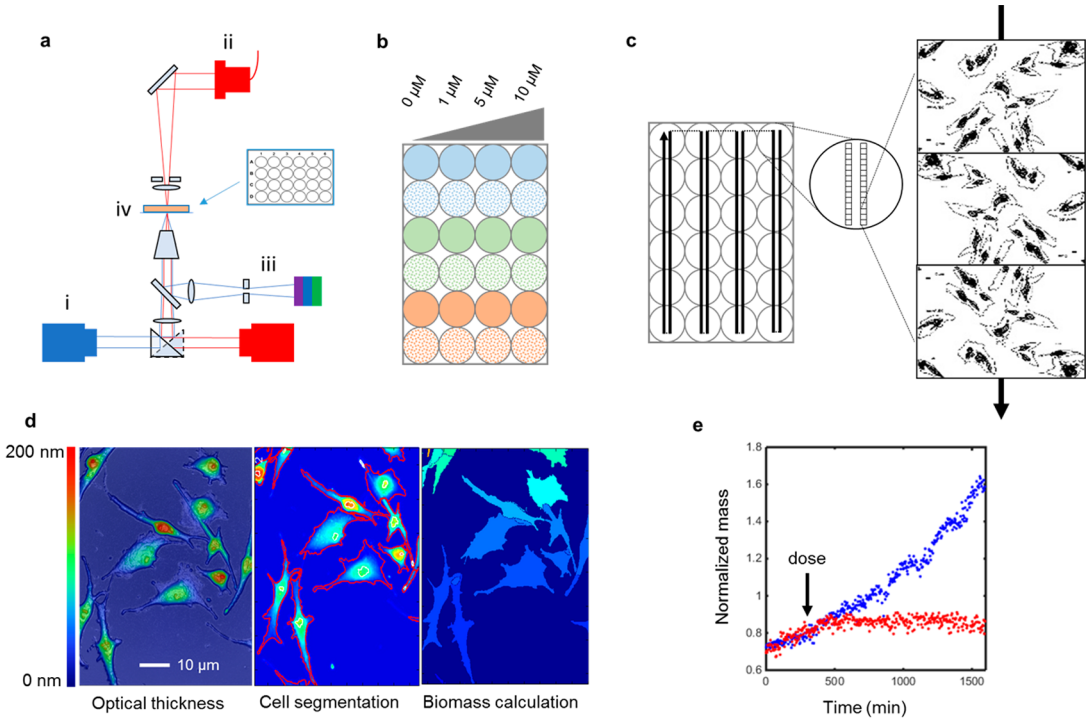

Figure 1. Schematic of HSLCI multiwell biomass accumulation assay. (a) The high-speed live-cell interferometry (HSLCI) system is configured with (i) a wide-field phase-detection camera, (ii) fiber-coupled light-emitting diode (LED) illumination source, and (iii) and fluorescence imaging capability (camera, filters, and illuminator). Motorized stages (iv) control $x-y$ motion of the sample above the microscope objective, while focus is automatically adjusted continuously by a piezo actuator coupled to the objective [10× Nikon Plan Fluorite, numerical aperture (NA) 0.3]. (b) Prior to imaging, cells and medium, including drug or vehicle, are dispensed into standard-format, glass-bottom multiwell plates. (c) During imaging, the sample plate is translated along each row of wells, collecting 30 images/well on each pass. Typical imaging time is 2 min/row of six wells. (d) Following collection, phase images are automatically analyzed in a custom pipeline that includes background flattening, cell detection and segmentation, and biomass calculation. (e) Individual cells are observed between images on the basis of their position, and biomass versus time plots are generated. Shown is a typical normalized mass vs time plot for single vemurafenib-sensitve (red) and vemurafenib-resistant (blue) cells.

and *PTEN*. Most of these mutations increase mitogen-activated protein kinase (MAPK) pathway signaling activity, which regulates cell proliferation, differentiation, and survival.[3−6] Targeted therapies, most notably against BRAF V600E and V600K activating mutations, has improved progression-free survival for many melanoma patients.[7] However, therapy resistance emerges in most cases of BRAF or MEK inhibitor monotherapy, often from preexisting or acquired mutations that reactivate the MAPK pathway downstream of the drug-targeted site.[8] Current BRAF and MEK inhibitor combination therapies aim to reduce the frequency of emergent resistance.[9,10] Drug selection guidance comes from clinical tumor staging, mutation screening, patient health, and prognostic factors such as lactate dehydrogenase levels.[11] Despite multifactorial guidance, resistance eventually develops for up to 80% of patients receiving combination therapy.[7] Genetic heterogeneity underlying mechanisms of preexisting and acquired resistance makes mutation screening incompletely predictive of drug susceptibility, both prior to the start of therapy and after the development of resistance, and increases the difficulty of selecting efficacious frontline and second-line therapies.[12−14]

Current efforts in repeat tumor assessment focus on noninvasive liquid biopsy methodologies such as the detection and analysis of circulating exosomes, microRNAs, circulating tumor DNA, circulating tumor cells, and proteomic profiling of serum proteins by mass spectrometry.[15,16] While samples from the circulation provide easily accessible materials that may be more representative of a patient's tumor heterogeneity than single-site tumor biopsies, there are presently no reliable molecular biomarkers from circulation sampling to guide targeted melanoma therapy or improve outcome predictions.[17−19] Other limitations include a lack of standardization, low sample yields, and the high cost of postisolation analyses, which makes many circulation-sampling methods impractical for broad-scale clinical implementations in their present state.[20,21]

An alternative to circulating biomarkers is in vitro measurement of drug responses in excised tumor cells by chemosensitivity assays, such as ATP quantification or assessments of cell metabolic activity.[22−25] Advocated by major cancer centers and international research organizations, such as the American Society of Clinical Oncology (ASCO), chemosensitivity assays have seen minimal adoption in melanoma treatment. This is mainly because of long, 3−7 day turnaround times that enable artifacts, a lack of supporting large-scale clinical trials, and poor compatibility with cancer heterogeneity due to the bulk, averaging nature of measurement methods.[26−29] A superior rapid, accurate, and inexpensive approach to determine melanoma drug sensitivity before and periodically during therapy is therefore desirable.

We have previously shown that optical interferometric microscopy provides an exciting potential solution by profiling drug-induced growth arrest in living single cells or cell clumps via changes in biomass over time with picogram sensitivity.[30,31] Like other quantitative phase imaging (QPI) modalities,[32,33]

DOI: 10.1021/acs.analchem.7b04828
Anal. Chem. 2018, 90, 3299−3306

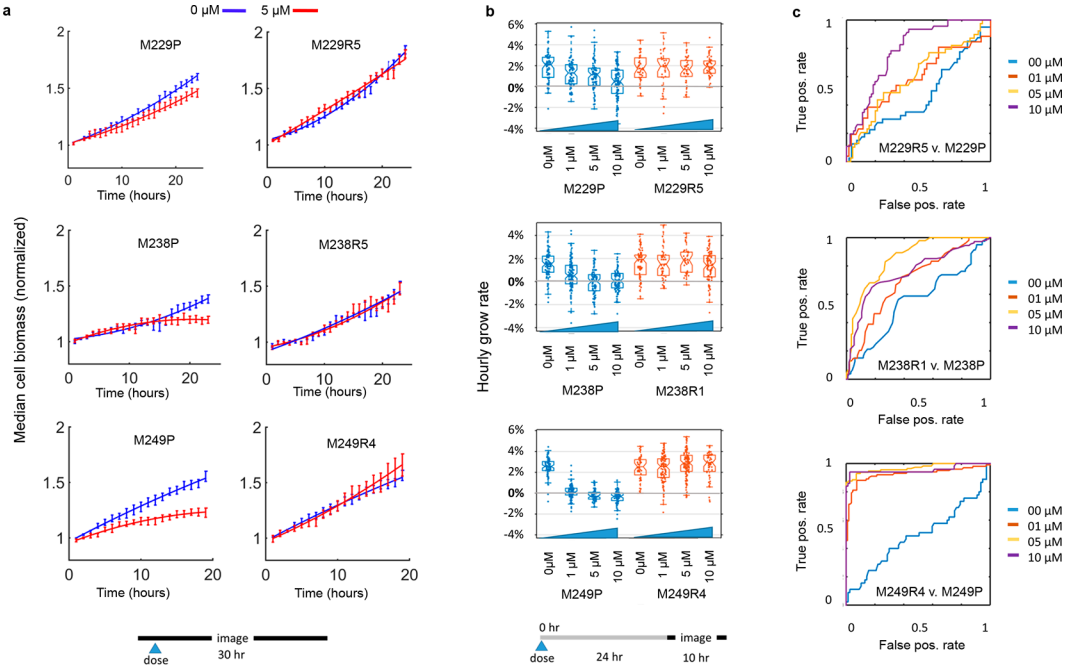

Figure 2. Biomass accumulation response to vemurafenib treatment. (a) Normalized population median biomass versus time plots of each melanoma line exposed to either 5 μM vemurafenib (red trace) or 0.1% dimethyl sulfoxide (DMSO, blue trace). Cells were synchronized prior to plating in glass-bottom dishes. Each sample was imaged for 3 h, after which either 0.1% DMSO (vehicle control) or 5 μM vemurafenib (treatment) was administered. After dosing, plates were imaged for 20−25 h by HSLCI under standard cell-culture conditions. Typical time between repeated measurements of the same location was 10−15 min. Each graph contains pooled data from four replicates. Error bars are ± standard error of measurement (SEM). (b) All six synchronized cell lines were plated into a single 24-well glass-bottom plate and dosed with either 0.1% DMSO or 1, 5, or 10 μM vemurafenib. After 24 h of incubation, the plate was imaged continuously for 10 h by HSLCI. Hourly growth rates were automatically calculated for individual cells in each sample by linear fit to the biomass versus time data. Data are from a single representative experiment (n = 3). Box-plot notches are 95% confidence intervals for the indicated medians. Each dot overlaid on a box plot represents the hourly growth rate of an individual cell. (c) Corresponding receiver operator characteristic (ROC) curves for data shown in panel b.

our technique is noninvasive and well-suited to this application due to its lack of fluorescence or dye labeling. However, our proof-of-principle work consisted of single-agent, small-scale studies of limited duration. The key remaining engineering challenge is to create a reliable platform for multiagent, multiconcentration parallel screens without sacrificing measurement accuracy or assay acceleration. Meeting this challenge requires, at a minimum, an order of magnitude increase in the number of different conditions tested within a single experiment and a corresponding increase in the number of individual cells analyzed per hour. This is a sizable hurdle, for a variety of methodological reasons, but is absolutely required to enable practical, rapid response profiling of patterns of drug resistance and intratumor heterogeneity and, ultimately, for development of a reproducible therapy selection method.

To reach this goal, we created an entirely new platform, utilizing industrial-grade imaging hardware and accelerated automated image analysis and data processing pipelines using low-cost, multicore PC processors and additional software improvements. Importantly, to achieve the required order-of-magnitude greater imaging throughput, we built the HSLCI around a different optical configuration than that used in all previous work. The new system consists of a custom inverted microscope equipped with a modified Shack−Hartman wavefront sensing camera (SID4BIO, Phasics, Inc.)[34] for rapid, vibration-insensitive cell mass measurements and a wide-field charge-coupled device (CCD) camera for correlative bright-field and fluorescence imaging (Figure 1). Dynamic focus stabilization enables continuous image collection over the entire sample area without pause. Stage-top or whole microscope enclosures provide long-term environment stability for imaging under physiology-approximating conditions (37 °C, 5% CO_2). The HSLCI captures images from standard-format, glass-bottom multiwell cell culture plates, and each well can contain a different cell type exposed to a unique drug dose or combination. The HSLCI experiments described here utilized 4- and 24-well glass bottom plates, although well counts of up to 96 are possible depending on the experimental conditions, including cell concentration, population sampling depth, required temporal resolution, and other parameters.

This present work describes a two-center study using HSLCI to quantify biomass kinetics for three isogenic sensitive/resistant pairs of patient-derived, ^{V600E}*BRAF* mutant melanoma cell lines in response to BRAF inhibitor (BRAFi), vemurafenib, and a battery of U.S. Food and Drug Administration (FDA)-approved kinase inhibitors. We show that HSLCI-quantified biomass kinetic signatures during 24 h of drug exposure discriminate between drug-sensitive and drug-resistant tumor subpopulations. HSLCI data are reproducible between study sites and consistent with longer multiday growth inhibition assays.

Of particular practical importance for any future clinical laboratory use is HSLCI's compatibility with presterilized, disposable, and standard-format multiwell sample plates. This enables efficient screening of multiple drugs and drug combinations in a single assay, simplifies sample handling, and avoids the need to sterilize and wash dedicated microfluidic components between runs.

DOI: 10.1021/acs.analchem.7b04828
Anal. Chem. 2018, 90, 3299−3306

RESULTS

Isogenic BRAF Inhibitor-Sensitive and -Resistant Melanoma Cell Lines. We evaluated three patient-derived ^{V600E}*BRAF* melanoma cell lines, M229P, M238P, and M249P, which are sensitive to the BRAFi, vemurafenib (IC_{50} < 1 μM), and their isogenic BRAFi-resistant sublines, M229R5, M238R1, and M249R4, created by vemurafenib coincubation over time (Table S1). M229R5 and M238R1 developed BRAFi resistance via epigenomic reprogramming, which is thought to occur in regressing or residual melanoma tumors from patients treated with MAPK inhibitor (MAPKi) therapy. This nongenomic evolution results in a MAPK-redundant form of resistance.[35] On the other hand, M249R4 acquired a ^{Q61K}*NRAS* mutation in addition to the ^{V600E}*BRAF* mutation. This concurrent *BRAF*/*NRAS* mutant configuration results in MAPK hyperactivation and a MAPK-addicted form of resistance, which is frequently detected during disease progression or with clinical relapses.[36−38] Thus, these pairs of cell lines represent pre- and post-treatment models of differential drug-sensitivity states that are clinically relevant; therefore, we used these lines to evaluate HSLCI performance in biomass profiling.

Biomass Kinetic Responses to Vemurafenib Exposure. Our previous work in breast cancer and multiple myeloma indicated that changes in the population median growth rates between sensitive and resistant cell lines is detectable with confidence within a few hours of drug exposure.[30,31] We also showed that the distribution of growth rates within a population is roughly Gaussian in both treated and control samples. There are no existing data for the rate of biomass change of BRAFi-sensitive or -resistant melanoma cells that grow as adherent single cells or clumps. Therefore, we measured the kinetics of vemurafenib response in the three paired, molecularly characterized melanoma lines using HSLCI, to establish rates and distributions of biomass change with or without drug exposure. First, we performed a standard multiday dose-escalation cell-counting assay to confirm sensitivity for the three parent and matched resistant lines at 1.0−10.0 μM vemurafenib exposure (Figure S1). As anticipated, the parental lines slowed and the matched resistant lines continued replicating with drug exposure. We next used 5 μM vemurafenib as the midpoint drug dose to measure the median population growth rate and cell mass by HSLCI for the six cell lines in the first 25 h of drug exposure, in order to quantify the average population kinetic response. (Figure 2a) Under these conditions, drug sensitivity of the M249P population was detectable as early as 6 h, while sensitivity of the M238P and M229P populations was detected at approximately 15 h. Significant growth rate reduction occurred in all three parental lines by 20 h. We observed significant natural variation in the growth rates of individual cells within each population, a result consistent with previous LCI studies. The distribution of single-cell hourly growth rates was typically symmetrical about the mean, with variation of roughly ±1% (standard deviation, SD) above and below the population mean. For example, plotting the M249P growth rate distribution obtained by HSLCI for each hour showed no change in the population median growth rate nor in the cellular growth rate distribution over the course of the 25 h experiment. (Figure S2a). In contrast, under the same conditions, 5 μM vemurafenib exposure showed population growth-rate heterogeneity and a decline below zero growth rate by about 15 h for >50% of cells (Figure S2b), indicative of the relative sensitivity of this line to the BRAF inhibitor. Similar temporal single-cell growth-rate distributions were seen in the other five cell lines, with kinetics proportional to the line's overall median sensitivity. These results were reproduced at both experimental sites with independently assembled HSLCI platforms.

By comparing the median cell mass of the vemurafenib-resistant melanoma lines to the mass of their isogenic, drug-sensitive parent lines, we found no consistent correlation between mass and resistance (Figure S3). This observation stands in contrast to a recent report of cell mass−drug resistance correlation in a mouse acute myeloid leukemia (AML) model, as measured by microfluidic devices.[39] However, that study did not compare isogenic paired sensitive and resistant tumor lines, and it remains to be determined whether or not mass itself is a useful metric of drug sensitivity.

The midpoint kinetic response data suggested that vemurafenib sensitivity, or lack thereof, would be distinguishable for all lines in a drug-escalation assay, as would be expected for cell counting, by measuring changes in sample growth rates after 24 h of drug exposure. To test this hypothesis and to examine the HSLCI methodology for multidose and multiagent screening, we collected short-term,10-h growth rate measurements of all three cell line pairs in parallel, at escalating vemurafenib doses, using a 24-well format. All six melanoma cell lines were dosed with 0.1% DMSO or 1, 5, or 10 μM vemurafenib. The parental lines (M229P, M238P, and M249P) showed a clear pattern of increasing growth inhibition at escalating drug concentrations, whereas the resistant lines (M229R5, M238R1, and M249R4) showed no growth inhibition over the drug dosing range compared to a vehicle DMSO control, consistent with cell-counting assays (Figure 2b).

Heterogeneity Quantification. We used receiver operator characteristic (ROC) analysis to determine the ability to distinguish individual resistant cells from sensitive cells, in an in silico mixture, by changes in their individual growth rates during exposure to vemurafenib (Figure 2c). This analysis indicated that cells from both M229P and M238P lines were distinguishable from their resistant derivative counterparts at vemurafenib doses of 5 μM [area under the curve (AUC) 0.60 and 0.85, respectively] and 10 μM (AUC 0.78 and 0.75, respectively). The M249P cells were the most sensitive to drug and were easily distinguishable on the basis of changes in growth rate, with AUC greater than 0.90 at vemurafenib doses of 1 μM and above.

We then deployed HSLCI to quantify the changes in growth rates of an actual mixed population of green fluorescent protein (GFP)-labeled M249R4 vemurafenib-resistant (M249R4-GFP) and unlabeled M249P vemurafenib-sensitive cells during drug exposure. Importantly, stable GFP expression in the M249R4 line did not significantly alter the growth rate distribution obtained by LCI for each hour of 5 μM vemurafenib exposure compared with unlabeled M249R4 cells (Figure S2c). Sensitive M249P and resistant M249R4-GFP cells grown together at a 1:1 ratio with 5 μM vemurafenib were imaged over 48 h (Figure 3a−c). In mixed culture, individual resistant cells were discriminated from sensitive cells on the basis of differences in growth rates (Figure 3d), and because the M249R4 cells were GFP-marked, they were easily identified relative to the unmarked M249P cells during the assay. Reproducibly, the population growth rate of M249R4 cells exceeded that of M249P cells, as expected, but each marked and unmarked population also showed outlier cells. A small percentage of

DOI: 10.1021/acs.analchem.7b04828
Anal. Chem. 2018, 90, 3299−3306

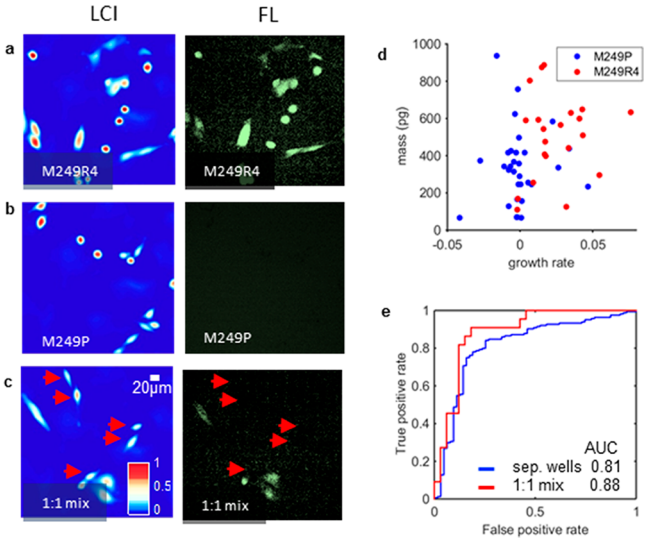

Figure 3. Detecting resistant cells in a mixed population. (a) Optical thickness (LCI, left) and in-register fluorescence images (FL, right) of M249R4-GFP vemurafenib-resistant cells. (b) LCI and fluorescence images of M249P vemurafenib-sensitive cells. (c) LCI and fluorescence images of a 1:1 mixture of M249P (red arrows, unlabeled) and M249R4 (labeled) cells. (d) Plot of biomass versus growth rate of a 1:1 M249P (blue)/M249R4-GFP (red) cell mixture exposed to 5 μM vemurafenib for 48 h. Cell identities are marked by fluorescence signals. (e) ROC curve classifying single sensitive versus resistant cells by their growth rates during exposure to 5 μM vemurafenib. The blue line is calculated from M229P and M249R4 cells imaged in separate wells, whereas the red line is calculated from a 1:1 cell mixture in the same wells (representative data are shown in panel d). Data shown are from a single representative experiment (n = 3–5).

M249R4-GFP cells showed zero to slightly negative growth rates, whereas a small percentage of M249P cells showed net-positive growth rates, revealing unanticipated vemurafenib-sensitive or -resistant outliers within each bulk population. As predicted from the in silico analysis, ROC analysis confirmed a high level of discrimination between sensitive and resistant melanoma cells (AUC 0.88), even when sensitive and resistant cells were combined in the same sample wells (Figure 3e). Similar trends were seen in 10:1 sensitive/resistant mixtures as well (Figure S4).

MEK Inhibitors with Vemurafenib-Resistant Melanoma. We performed rapid HSLCI dose–response assays in triplicate, using a panel of three FDA-approved and two investigational kinase inhibitors tested in clinical trials for treating metastatic melanoma, to simulate selection of salvage therapy for patients who develop resistance to front-line vemurafenib (Figure 4). One inhibitor in the panel targets BRAF, whereas the other four target MEK1 or MEK1/2 (Table S2). We selected M249R4 cells for study because of their robust growth profile and strong resistance to vemurafenib. Figure 4 shows typical results from two individual experimental runs, while Figure S5 shows results from all repeats fitted to a sigmoidal dose–response function for reference. Control DMSO-treated cells exhibited a median growth rate of ~2.5%·h^{-1} at 0.1% DMSO concentration (v/v), decreasing slightly to 2%·h^{-1} at higher concentrations (0.3%–0.5% v/v). For each targeted kinase inhibitor, the peak tolerated serum concentration (C_{max}, nanograms per milliliter), as measured in clinical trials, is shown on the dose–response curves by an

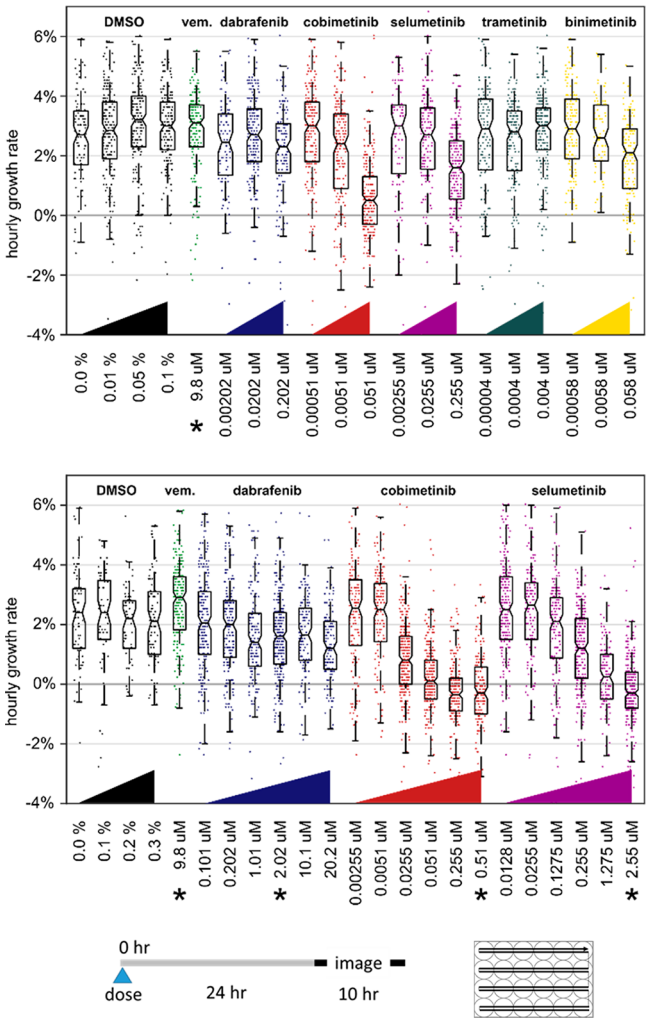

Figure 4. Effects of five kinase inhibitors on vemurafenib-resistant melanoma measured by HSLCI. M249R4 cells were plated into 24-well plates and dosed at increasing concentrations of each inhibitor. After 24 h of incubation, the plate was imaged by HSLCI continuously for 10 h. Typically four different doses for each inhibitor, and four DMSO controls, were measured in each run simultaneously. Data in the figure represent two typical experimental runs, using different dose gradations. Hourly growth rates were automatically calculated for individual cells in each sample by linear fit to the biomass vs time data. Each box plot summarizes the hourly growth rates of a population of cells exposed to escalating concentrations of each drug. Individual dots in the underlying scatter plots represent the growth rates of single cells. Box-plot notches are indicative of 95% confidence intervals for the medians. Median number of cells per well: top panel 159 (range 79–216); bottom panel 160 (range 59–294).

asterisk (*). (See Supporting Information for details of C_{max} determination.) As expected for this highly vemurafenib-resistant line, the BRAF inhibitor dabrafenib showed no growth inhibition as compared to the DMSO control. The MEK1 inhibitor cobimetinib and the MEK1/2 inhibitor trametinib were the most effective growth inhibitors: cobimetinib completely arrested median sample growth at 0.255 μM concentration, which is roughly half of the maximum tolerated serum concentration, while trametinib arrested growth at a concentration between 4 and 40 nM, or between 0.1× and 1× C_{max}. MEK1/2 inhibitor selumetinib arrested growth at 2.55 μM, equal to 1× C_{max}, while MEK1 inhibitor binimetinib failed to halt growth at concentrations below 2.91 μM, or 5× C_{max},

DOI: 10.1021/acs.analchem.7b04828
Anal. Chem. 2018, 90, 3299–3306

suggesting that binimetinib would be an unlikely candidate for salvage therapy in this simulated case.

DISCUSSION

Here we demonstrated the ability of a rapid HSLCI platform to quantify individual cell drug sensitivity in tumor cell populations. This quantification may provide critical data for treatment selections on a whole-tumor population level and can identify specific subpopulation drug sensitivities to predict drug resistance at a single-cell level. Furthermore, concordant data obtained from two institutions with independently constructed and standardized HSLCI platforms highlights the reproducibility of two similar but distinct implementations. This two-center study design is unique among live-cell response profiling approaches and provides confidence that the newly configured HSLCI has the required consistency to warrant further development as a clinically useful approach.

In comparison to other single-live-cell biomass profiling approaches,[33,40,41] including our own prior interference microscopic studies,[30] HSLCI represents a substantial technical advance in single-cell sampling throughput, cell-tracking duration, and parallel measurement of multiple agents. For example, Stevens et al.[39] recently used microchannel resonators to demonstrate that the combined measurement of single-cell mass and growth rates could be used identify drug-resistant cells isolated from an engineered mouse AML model. Their high-throughput "next-gen" system with 12 microresonators could measure up to 60 cells/hour, where cells are measured serially, each for 15 min, resulting in simple snapshots in time. Unfortunately, tumors that grow in small clusters or clumps, as do many melanoma samples, are inaccessible to this platform unless they are disaggregated, which affects their growth characteristics and drug sensitivity.

In contrast, HSLCI typically measures between 10^3 and 10^4 cells in each experiment across a total area greater than 700 mm^2, tracking each cell individually for hours to days, and is well-suited to tumors that grow in clusters or clumps without disaggregation. In addition, identifying rare resistant clones in a population of normal or therapy-sensitive malignant cells requires such deep sampling. For instance, typical minimal residual disease detection by multicolor flow cytometry requires sampling to a depth of at least 10^4 and up to 10^6 cells.[42] We believe that realistic improvements may allow HSLCI throughput to approach 10^5 cells/experiment.

Quantitative phase imaging (QPI) techniques have proven to be versatile alternatives for measuring single-cell mass, especially in tumors that grow in clusters or clumps, without a need for disaggregation. Examples include measuring cell growth and death, membrane mechanics, wound healing, and cytotoxicity and detecting circulating tumor cells.[32,43−48] However, current QPI implementations utilized for longitudinal biomass tracking are significantly limited by low throughput, measuring only several hundred cells simultaneously in areas of less than 10 mm^2.[43,45] To date, maximum published durations of other continuous, longitudinal, QPI-based single-cell experiments are 48 h or less. An exception appears to be a study by Li et al.[49] of treatment responses in tumor models, which was conducted for 240 h. However, this study was notably not automated, requiring manual removal of samples from an incubator every 24 h, and suffered from poor temporal resolution (10-image snapshots per day per sample). Due to the mechanical and environmental stability of the HSLCI system, we have been able to track single cells and cell clusters for more than 5 days, with no time limit yet found. This is a dramatic increase over our previous 12-h maximum duration interference microscopic work and enables the study of behaviors that evolve over many minutes, hours, or days, encompassing the vast majority of cellular responses. Cell observation duration is of direct relevance to detecting drug responses in cells isolated from patients, as it is necessary to distinguish between growth arrest (cytostasis) and death resulting from drug exposure versus other influences. With HSLCI this is accomplished by repeatedly observing individual cells before and after drug exposure-response, a process that requires several hours or more.

The primary drawback of HSLCI compared to microscopic, single-cell snapshot fluorescent assays and microresonator mass assays is the relatively large data footprint and extensive image analysis required to generate a biologically interpretable result. At present, data analysis time, not hardware capability, is throughput-limiting. On the other hand, the single-cell images generated by HSLCI are inherently information-rich, allowing not only mass accumulation but also cytokinesis, motility, and cell-shape information to be quantified. Integrating these mutually supporting metrics will be a direction for future research. Furthermore, system upgrades can be largely accomplished by software rather than hardware modifications, making the upgrade path efficient and flexible. Fast cell mass measurement by phase imaging would be complementary to high-content screening systems based on automated confocal fluorescence microscopy. Finally, on the basis of our results, it is likely that other forms of interference microscopy can be similarly adapted to enable faster measurement speeds.

METHODS

Cell Lines. M229P, M229R5, M238P, M238R1, M249P, and M249R4 cell lines were grown in Dulbecco's modified Eagle's medium (DMEM), high glucose with 10% heat-inactivated fetal bovine serum (FBS) (Omega Scientific) and 2 mM glutamine in a 37 °C, humidified, 5% CO_2 incubator. M229R5, M238R1, and M249R4 cells were exposed to 1 μM vemurafenib every 2−3 days. Cell counting from 6-well plates with controls and a range of vemurafenib concentrations was performed for 5 days following overnight seeding.

Population Kinetic Response Experiments. Cells were synchronized by growing to confluence in 75 mL tissue culture flasks and collected by a shake-off technique. Cells were plated at 1×10^5 cells/mL in 25 mm dishes and incubated overnight. Prior to imaging, samples were equilibrated thermally for 1 h on the microscope stage and then imaged for 3 h, after which either 0.1% DMSO vehicle control or 5 μM vemurafenib was administered and dishes were waimaged for another 25−30 h.

Vemurafenib Dose−Response Experiments. Cells were first synchronized by shake-off, each of the six melanoma cell lines was seeded into four wells each of a 24-well glass bottom plate at 1×10^5 cells/mL, and the plates were incubated overnight. Each line was dosed with 0.1% DMSO carrier control, or 1, 5, or 10 μM vemurafenib. Cells were incubated for 24 h, and then the entire plate was imaged by HSLCI for 10 h.

Fluorescence Mixing Experiments. M249P and M249R4-GFP (1.25×10^4 cells each) were added together in a total volume of 1 mL tissue culture medium. A portion (0.7 mL) of the mixture was dispensed into each well of an Ibidi 4-well Ph+ μ-slide. Cells settled over 6 h, after which 5 μM vemurafenib was added to each well. Ibidi oil sealed the liquid

DOI: 10.1021/acs.analchem.7b04828
Anal. Chem. 2018, 90, 3299−3306

opening of each well before the plate was placed onto the LCI stage. All wells were imaged continuously for 48 h. Fluorescence images were taken with a Hamamatsu EM CCD camera (C9100-02 EMCCD) serially after every five phase-imaging loops were completed. Green fluorescence was captured by use of a 38 HE green fluorescent filter set (Zeiss) with an excitation wavelength of 450−490 nm, a beamsplitter wavelength of 496 nm, and an emission wavelength of 500−550 nm. Fluorescence excitation was provided by an X-Cite 120Q wide-field fluorescence microscope excitation light source (Excelitas).

Kinase Inhibitor Panel Assay. M249R4 cells were plated in a 24-well optical glass-bottomed plate (catalog no. P24-0-N, Cellvis) at 1×10^4 cells/mL (total of 1 mL in each of 24 wells) in medium (DMEM with 10% FBS and 2 mM L-glutamine) containing 1 μM vemurafenib. Plated cells were allowed to adhere overnight at 37 °C in 5% CO_2. All cells were washed with 1× phosphate-buffered saline, pH 7.4, and provided with fresh medium. Immediately following washing and feeding, cells were dosed with inhibitors at dose-escalating concentrations and incubated under standard cell-culture conditions for 24 h. After incubation, cells were imaged for 10 h by use of the HSCLI system.

■ ASSOCIATED CONTENT

Supporting Information

The Supporting Information is available free of charge on the ACS Publications website at DOI: 10.1021/acs.analchem.7b04828.

Five figures showing 7-day proliferation assay, distributions of single-cell growth rates over time, relative mass comparison between isogenic lines, detection of minority resistant cells in a mixed population, and dose−response curves; two tables listing patient-derived melanoma lines and kinase inhibitor dosing; additional text describing high-speed live-cell interferometry, image analysis, HSLCI platform performance metrics, cell generation, drug sourcing and preparation, kinase inhibitor 1× dose determination, and cell proliferation assay (PDF)

■ AUTHOR INFORMATION

Corresponding Authors

*E-mail mteitell@ucla.edu.
*E-mail jreed@vcu.edu.

ORCID

Thomas A. Zangle: 0000-0001-5899-3517
Jason Reed: 0000-0002-3314-8699

Author Contributions

D.H. and K.A.L. contributed equally. J.R. and M.A.T. conceived the concept and planned the study, with input from R.S.L. D.H., K.A.L., O.Y., D.G., I.J.R., M.P., G.M., and T.A.Z. carried out the experiments and analyzed the data. J.R., M.A.T., D.H., and K.A.L. cowrote the paper.

Notes

The authors declare no competing financial interest.

■ ACKNOWLEDGMENTS

Funding for this work was provided by National Institutes of Health Grant R01CA185189 to J.R. and M.A.T. and, in part, with funding from NCI Cancer Center Support Grant P30 CA016059 to Massey Cancer Center.

■ REFERENCES

(1) Siegel, R. L.; Miller, K. D.; Jemal, A. *Ca-Cancer J. Clin.* **2017**, *67*, 7−30.
(2) Rogers, H. W.; Weinstock, M. A.; Feldman, S. R.; Coldiron, B. M. *JAMA Dermatol.* **2015**, *151*, 1081−1086.
(3) Kunz, M.; Holzel, M. *Cancer Metastasis Rev.* **2017**, *36*, 53−75.
(4) Zhang, T.; Dutton-Regester, K.; Brown, K. M.; Hayward, N. K. *Pigm. Cell Melanoma Res.* **2016**, *29*, 266−283.
(5) Eskiocak, B.; McMillan, E.; Mendiratta, S.; Kollipara, R.; Zhang, H.; Humphries, C.; Wang, C.; Garcia-Rodriguez, J.; Ding, M.; Zaman, A.; Rosales, T.; Eskiocak, U.; Smith, M. P.; Sudderth, J.; Komurov, K.; DeBerardinis, R. J.; Wellbrock, C.; Davies, M. A.; Wargo, J. A.; Yu, Y.; et al. *Cancer Discovery* **2017**, *7*, 832−851.
(6) Shtivelman, E.; Davies, M. Q.; Hwu, P.; Yang, J.; Lotem, M.; Oren, M.; Flaherty, K. T.; Fisher, D. E. *Oncotarget* **2014**, *5*, 1701−1752.
(7) Welsh, S. J.; Rizos, H.; Scolyer, R. A.; Long, G. V. *Eur. J. Cancer* **2016**, *62*, 76−85.
(8) Inamdar, G. S.; Madhunapantula, S. V.; Robertson, G. P. *Biochem. Pharmacol.* **2010**, *80*, 624−637.
(9) Luke, J. J.; Flaherty, K. T.; Ribas, A.; Long, G. V. *Nat. Rev. Clin. Oncol.* **2017**, *14*, 463−482.
(10) Simeone, E.; Grimaldi, A. M.; Festino, L.; Vanella, V.; Palla, M.; Ascierto, P. A. *BioDrugs* **2017**, *31*, 51−61.
(11) Spagnolo, F.; Ghiorzo, P.; Orgiano, L.; Pastorino, L.; Picasso, V.; Tornari, E.; Ottaviano, V.; Queirolo, P. *OncoTargets Ther.* **2015**, *8*, 157−168.
(12) Ahronian, L. G.; Corcoran, R. B. *Genome Med.* **2017**, *9*, 37.
(13) Wagle, N.; Emery, C.; Berger, M. F.; Davis, M. J.; Sawyer, A.; Pochanard, P.; Kehoe, S. M.; Johannessen, C. M.; Macconaill, L. E.; Hahn, W. C.; Meyerson, M.; Garraway, L. A. *J. Clin. Oncol.* **2011**, *29*, 3085−3096.
(14) Bedard, P. L.; Hansen, A. R.; Ratain, M. J.; Siu, L. L. *Nature* **2013**, *501*, 355−364.
(15) Huang, S. K.; Hoon, D. S. *Mol. Oncol.* **2016**, *10*, 450−463.
(16) Ulz, P.; Heitzer, E.; Geigl, J. B.; Speicher, M. R. *Int. J. Cancer* **2017**, *141*, 887−896.
(17) Siravegna, G.; Marsoni, S.; Siena, S.; Bardelli, A. *Nat. Rev. Clin. Oncol.* **2017**, *14*, 531−548.
(18) De Luca, F.; Rotunno, G.; Salvianti, F.; Galardi, F.; Pestrin, M.; Gabellini, S.; Simi, L.; Mancini, I.; Vannucchi, A. M.; Pazzagli, M.; Di Leo, A.; Pinzani, P. *Oncotarget* **2016**, *7*, 26107−26119.
(19) Klinac, D.; Gray, E. S.; Millward, M.; Ziman, M. *Front. Oncol.* **2013**, *3*, 54.
(20) Gold, B.; Cankovic, M.; Furtado, L. V.; Meier, F.; Gocke, C. D. *J. Mol. Diagn.* **2015**, *17*, 209−224.
(21) Cree, I. A. *J. Controlled Release* **2013**, *172*, 405−409.
(22) Singer, C. F.; Klinglmuller, F.; Stratmann, R.; Staudigl, C.; Fink-Retter, A.; Gschwantler, D.; Helmy, S.; Pfeiler, G.; Dressler, A. C.; Sartori, C.; Bilban, M. *PLoS One* **2013**, *8*, No. e66573.
(23) Haglund, C.; Aleskog, A.; Nygren, P.; Gullbo, J.; Hoglund, M.; Wickstrom, M.; Larsson, R.; Lindhagen, E. *Cancer Chemother. Pharmacol.* **2012**, *69*, 697−707.
(24) Bellot, G. L.; Tan, W. H.; Tay, L. L.; Koh, D.; Wang, X. *J. Cancer Res. Clin. Oncol.* **2012**, *138*, 463−482.
(25) Wiberg, K.; Carlson, K.; Aleskog, A.; Larsson, R.; Nygren, P.; Lindhagen, E. *Med. Oncol. (N. Y., NY, U. S.)* **2009**, *26*, 193−201.
(26) Franken, N. A.; Rodermond, H. M.; Stap, J.; Haveman, J.; van Bree, C. *Nature protocols* **2006**, *1*, 2315−2319.
(27) Kurbacher, C. M.; Cree, I. A. *Methods in molecular medicine* **2005**, *110*, 101−120.
(28) Whitehouse, P. A.; Knight, L. A.; Di Nicolantonio, F.; Mercer, S. J.; Sharma, S.; Cree, I. A. *Anti-Cancer Drugs* **2003**, *14*, 369−375.
(29) Wu, B.; Zhu, J. S.; Zhang, Y.; Shen, W. M.; Zhang, Q. *World journal of gastroenterology* **2008**, *14*, 3064−3068.
(30) Reed, J.; Chun, J.; Zangle, T. A.; Kalim, S.; Hong, J. S.; Pefley, S. E.; Zheng, X.; Gimzewski, J. K.; Teitell, M. A. *Biophys. J.* **2011**, *101*, 1025−1031.

DOI: 10.1021/acs.analchem.7b04828
Anal. Chem. 2018, 90, 3299−3306

(31) Chun, J.; Zangle, T. A.; Kolarova, T.; Finn, R. S.; Teitell, M. A.; Reed, J. *Analyst* **2012**, *137*, 5495−5498.
(32) Kuhn, J.; Shaffer, E.; Mena, J.; Breton, B.; Parent, J.; Rappaz, B.; Chambon, M.; Emery, Y.; Magistretti, P.; Depeursinge, C.; Marquet, P.; Turcatti, G. *Assay Drug Dev. Technol.* **2013**, *11*, 101−107.
(33) Bettenworth, D.; Bokemeyer, A.; Poremba, C.; Ding, N.; Ketelhut, S.; Lenz, P.; Kemper, B. *Histol. Histopathol.* **2017**, 11937.
(34) Bon, P.; Maucort, G.; Wattellier, B.; Monneret, S. *Opt. Express* **2009**, *17*, 13080−13094.
(35) Song, C.; Piva, M.; Sun, L.; Hong, A.; Moriceau, G.; Kong, X.; Zhang, H.; Lomeli, S.; Qian, J.; Yu, C. C.; Damoiseaux, R.; Kelley, M. C.; Dahlman, K. B.; Scumpia, P. O.; Sosman, J. A.; Johnson, D. B.; Ribas, A.; Hugo, W.; Lo, R. S. *Cancer Discovery* **2017**, *7*, 1248−1265.
(36) Shi, H. B.; Hugo, W.; Kong, X. J.; Hong, A.; Koya, R. C.; Moriceau, G.; Chodon, T.; Guo, R. Q.; Johnson, D. B.; Dahlman, K. B.; Kelley, M. C.; Kefford, R. F.; Chmielowski, B.; Glaspy, J. A.; Sosman, J. A.; van Baren, N.; Long, G. V.; Ribas, A.; Lo, R. S. *Cancer Discovery* **2014**, *4*, 80−93.
(37) Moriceau, G.; Hugo, W.; Hong, A.; Shi, H. B.; Kong, X. J.; Yu, C. C.; Koya, R. C.; Samatar, A. A.; Khanlou, N.; Braun, J.; Ruchalski, K.; Seifert, H.; Larkin, J.; Dahlman, K. B.; Johnson, D. B.; Algazi, A.; Sosman, J. A.; Ribas, A.; Lo, R. S. *Cancer Cell* **2015**, *27*, 240−256.
(38) Hugo, W.; Shi, H. B.; Sun, L.; Piva, M.; Song, C. Y.; Kong, X. J.; Moriceau, G.; Hong, A. Y.; Dahlman, K. B.; Johnson, D. B.; Sosman, J. A.; Ribas, A.; Lo, R. S. *Cell* **2015**, *162*, 1271−1285.
(39) Stevens, M. M.; Maire, C. L.; Chou, N.; Murakami, M. A.; Knoff, D. S.; Kikuchi, Y.; Kimmerling, R. J.; Liu, H. Y.; Haidar, S.; Calistri, N. L.; Cermak, N.; Olcum, S.; Cordero, N. A.; Idbaih, A.; Wen, P. Y.; Weinstock, D. M.; Ligon, K. L.; Manalis, S. R. *Nat. Biotechnol.* **2016**, *34*, 1161−1167.
(40) Popescu, G.; Park, Y.; Lue, N.; Best-Popescu, C.; Deflores, L.; Dasari, R. R.; Feld, M. S.; Badizadegan, K. *Am. J. Physiol Cell Physiol* **2008**, *295*, C538−544.
(41) Godin, M.; Delgado, F. F.; Son, S.; Grover, W. H.; Bryan, A. K.; Tzur, A.; Jorgensen, P.; Payer, K.; Grossman, A. D.; Kirschner, M. W.; Manalis, S. R. *Nat. Methods* **2010**, *7*, 387−390.
(42) van Dongen, J. J. M.; van der Velden, V. H. J.; Bruggemann, M.; Orfao, A. *Blood* **2015**, *125*, 3996−4009.
(43) Mir, M.; Bergamaschi, A.; Katzenellenbogen, B. S.; Popescu, G. *PLoS One* **2014**, *9*, No. e89000.
(44) Pavillon, N.; Kuhn, J.; Moratal, C.; Jourdain, P.; Depeursinge, C.; Magistretti, P. J.; Marquet, P. *PLoS One* **2012**, *7*, No. e30912.
(45) Bettenworth, D.; Lenz, P.; Krausewitz, P.; Bruckner, M.; Ketelhut, S.; Domagk, D.; Kemper, B. *PLoS One* **2014**, *9*, No. e107317.
(46) Zlotek-Zlotkiewicz, E.; Monnier, S.; Cappello, G.; Le Berre, M.; Piel, M. *J. Cell Biol.* **2015**, *211*, 765−774.
(47) Singh, S. P.; Kang, S.; Kang, J. W.; So, P. T. C.; Dasari, R. R.; Yaqoob, Z.; Barman, I. *Sci. Rep.* **2017**, *7*, No. 10829.
(48) Singh, D. K.; Ahrens, C. C.; Li, W.; Vanapalli, S. A. *Lab Chip* **2017**, *17*, 2920−2932.
(49) Li, Y. Y.; Petrovic, L.; La, J.; Celli, J. P.; Yelleswarapu, C. S. *J. Biomed. Opt.* **2014**, *19*, No. 116001.

DOI: 10.1021/acs.analchem.7b04828
Anal. Chem. 2018, 90, 3299−3306